Received: 1 February 2021 | Revised: 26 March 2021 | Accepted: 15 April 2021

DOI: 10.1002/jhet.4284

ARTICLE

JOURNAL OF HETEROCYCLIC CHEMISTRY WILEY

Crystal structure and quantum chemical calculations of (*E*)1-benzyl-3-((4-methoxyphenyl)imino)-5-methylindolin-2-one

Hend A. A. Abdel El-wahab[1] | **Ahmed K. Hamdy**[1] | **Carola Schulzke**[2] | **Tarek Aboul-Fadl**[1] | **Wesam S. Qayed**[1]

[1]Department of Medicinal Chemistry, Faculty of Pharmacy, Assuit University, Assuit, Egypt

[2]Institut für Biochemie, Universität Greifswald, Greifswald, Germany

Correspondence
Carola Schulzke, Institut für Biochemie, Universität Greifswald, Felix-Hausdorff-Straße 4, 17489 Greifswald, Germany.
Email: carola.schulzke@uni-greifswald.de

Abstract

The known Schiff base compound, (*E*)1-benzyl-3-((4-methoxyphenyl)imino)-5-methylindolin-2-one, was prepared as before by reacting 1-benzyl-5-methylindoline-2,3-dione with 4-methoxyaniline. The product was unambiguously characterized using elemental analysis, ^{1}H and ^{13}C-NMR spectroscopy, and its new single-crystal X-ray structural analysis. Molecular orbital calculations were conducted in order to investigate the structures and relative stabilities of the (*E*) and (*Z*) isomers of 1-benzyl-3-([4 methoxyphenyl]-imino)-5-methylindolin-2-one. Specific attention was paid to the (*E*) isomer. The available crystallographic experimental data for the latter ensured also validation of the model structures computationally derived at the theoretical B3LYP/6-31G(d,p) level.

1 | INTRODUCTION

1H-indole-2,3-dione and derivatives thereof are frequently used as precursors for the synthesis of important classes of heterocyclic drugs. According to a literature survey, Schiff and Mannich bases of 1H-indole-2,3-diones exhibit rather broad and very diverse pharmacological activities including those against cancer, bacteria, and fungi, as well as antidiabetic, anticonvulsant, antitubercular, anti-HIV, neuroprotective [1], antioxidant [2], antiglycation [3], antimalarial [4], antiinflammatory, analgesic [5], and antianxiety effects [6]. Consequently, the attractive properties of Schiff and Mannich bases, including biological ones, and their general chemical as well as their specific molecular structures have already been analyzed for a considerable period of time [7].

The distinct chemical structure of any molecule profoundly affects its biological properties, irrespective of the chemical class that it belongs to. In this context, computational chemistry has a crucial role in the fields of chemical, biological, and material sciences. In organic chemistry, it helps understanding concepts, for example, regarding the molecular structure and explaining reaction pathways and chemical mechanisms through the estimation of compounds' geometrical properties [8]. It may also deliver fine details of the electronic properties of reactants, intermediates, and products as well as support and explain various experimental observations [9,10]. The still growing interlocking of experimental and computational chemistry has solved a wide range of organic chemical problems. Computational chemistry might even encourage novel ideas in planning unprecedented chemical reactions and experimental mechanistic studies[1,11,12].

Here, crystallographic evaluation and quantum chemical calculation of the molecular metrical parameters and the computational structures at the atomic level, that is,

combined experimental and in silico studies, are reported and discussed in relation based on a newly crystallized known indole derivative. The structural behavior of the molecule as embedded in the solid crystal lattice is compared with the corresponding gas phase structure providing notable insights in particular with respect to the experimentally observed formation and computed relative stability of (*E*) versus (*Z*) isomers.

2 | RESULTS AND DISCUSSION

2.1 | Description of the crystal structure

The unit cell of the title compound I bears 16 molecules while the crystal system is orthorhombic with the space group *Fdd*2. All molecules are present as the compound's (*E*) isomer (Figure 1). The N2-C2 distance between indole ring and bridging Schiff base nitrogen with 1.280(5) Å falls within the range of a typical C═N double bond, while the N2-C17 distance between the bridging nitrogen and the phenyl ring of 1.419(4) Å clearly suggests a C—N single bond like in other Schiff base compounds. The bond angles involving the Schiff base nitrogen, that is, N2-C2-C1, N2-C2-C3, and C2-N2-C17 are 118.6(3)°, 136.0 (3)°, and 120.7(3)°, respectively, and they are agreeing with an sp^2 hybrid character for both C2 and N2 atoms. The indole 5-ring plane (N1, C1, C2, C3, C8) is nearly perpendicular to the plane of the phenyl ring C11–C16 with a torsion angle of C1-N1-C10-C11 of −92.3(4)°. C2 of the indole moiety is linked through the Schiff base functional group to a second phenyl ring C17–C22 which is twisted into the opposite direction relative to indole with a torsion angle of C22-C17-N2-C2 at 75.0(5)° [6].

The molecular structure exhibits a weak intramolecular nonclassical hydrogen bond between the phenyl carbon C16 as a donor and the keto oxygen atom as an acceptor (d D-H 0.95 Å; d H···A 2.68 Å, D···A 3.431 Å, < DHA 137°). In the crystal lattice, one significant intermolecular nonclassical hydrogen bonding interaction is present (C18—H18···$N2^{i}$; [i] -x + 3/2, −y + 1/2, z) with distances d (D-H), d (H···A), d (D···A) of 0.95 Å, 2.65 Å, and 3.511(5) Å, respectively, and an angle < (DHA) of 151°. This interaction is bi-directional ($R_2^2(8)$ pattern) and leads to the formation of hydrogen bonded dimers. The dimers are further stabilized by π-π stacking of the phenyl rings of the indole moieties with a centroid-to-centroid distance of 3.672(2) Å and a slippage of 1.482 Å. Adjacent dimers in b or in c direction are arranged in parallel orientation while those in c direction are perpendicular. This leads to a type of zig-zag fashion arrangement when viewed along the crystallographic c-axis (Figure 2). All methoxy-substituted phenyl rings are arranged in the same direction with regard to the c-axis, that is, here shown as below the rest of the molecules/dimers (Figure 3) and those of adjacent (in b direction) molecules point away from each other based on the fact that the molecules constitute (*E*) isomers. The orientation of the methoxy-phenyl moiety is further supported by the hydrogen bond involving N2 to which it is attached plus O1 as acceptors and C6-H6 as donor. This hydrogen bond draws an adjacent molecule near and prevents the methoxy-phenyl moiety to bend over for a lack of space. Based on the observed intra- and intermolecular interactions, it is certainly reasonable why only the (*E*) isomer was observed crystallographically, but it is not entirely exclusive. A full interaction map (FIM; see Figure S8) analysis reveals that only the hydrogen bonding interaction of N2 and O1 as acceptors with C6-H6 as a donor can be considered exemplary geometry wise, and this only indirectly involves the orientation of the methoxy-phenyl substituent. All other inter- or intramolecular interactions are far from geometrically ideal compared to other structures in the Camdridge Crystallographic Database, that is, also with the (*Z*) isomer-related intermolecular interactions are presumed to be generally possible. It is, hence, impossible based on the crystallographic data alone to elucidate whether the preference for the (*E*) isomer is an intrinsic feature of the molecule itself or whether this is driven by crystal packing effects. Therefore, in order to understand in more detail why only the (*E*) isomer crystallized, a comprehensive computational investigation into this issue was carried out.

2.2 | Computational studies

DFT methods were used to calculate selected geometrical parameters. The respective calculations were initially based on the experimentally observed metrical parameters. The findings of computational DFT and experimental XRD methods are very similar showing merely minor deviations, that may attribute to the molecular environment differences. The experimental molecular structure of the (*E*) isomer of the title compound was characterized by X-ray crystallography, that is, necessarily in the crystalline phase, whereas DFT calculations of the isolated molecule and the second isomer were performed in the gas phase. Geometrical parameters calculated for the (*E*) isomer (Figure 1) together with the experimental data of the title compound are summarized in Tables 1–3. The observed differences can be assigned predominantly to packing effects and intermolecular interactions reflected in the experimental data. Notably in the X-ray structure, the double bonds are shorter and thereby appear to be a little less delocalized in comparison.

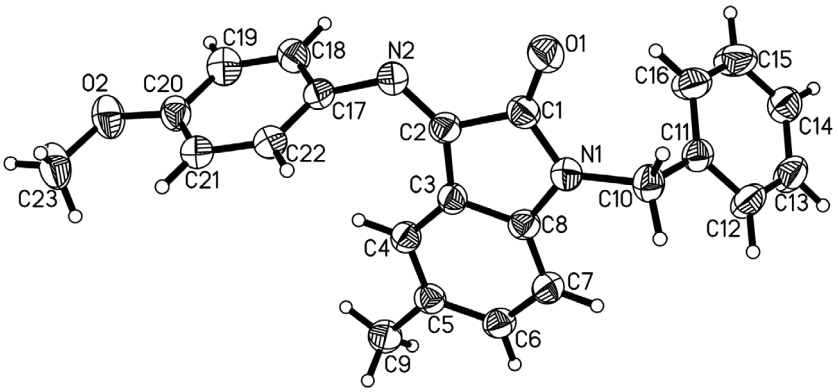

FIGURE 1 The molecular structure of compound I. Ellipsoids are shown at the 50% probability level

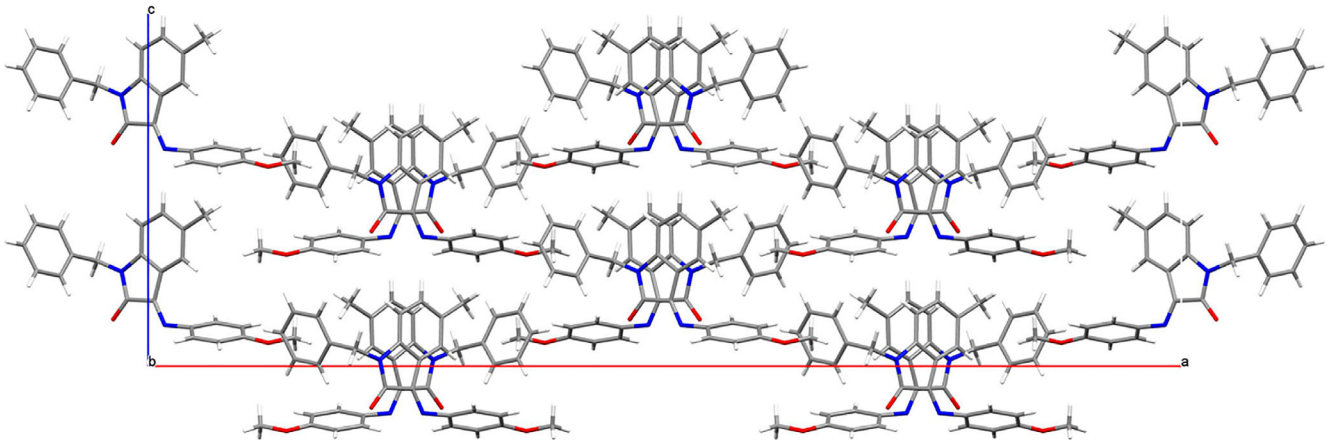

FIGURE 2 FCrystal packing of compound (I) along the c-axis [Color figure can be viewed at wileyonlinelibrary.com]

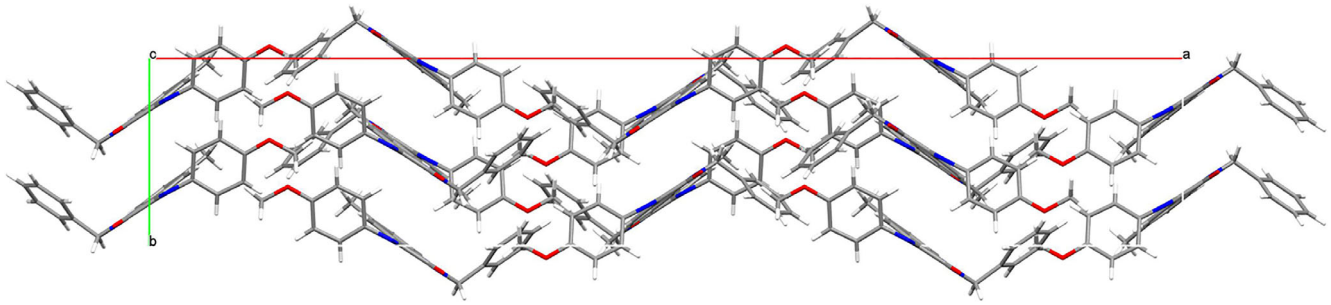

FIGURE 3 Crystal packing of compound (I) along the b-axis [Color figure can be viewed at wileyonlinelibrary.com]

2.2.1 | Mulliken atomic charges

In order to understand the electronic structure of the molecule better, Mulliken charges were computed [13,14], and the results are listed in Table 4. The charge distribution across the atoms was found to be significant in describing donor and acceptor pairs and to obtain insights into the overall chemical activity of the compound. The calculations are also represented in form of the MEP surfaces in Figure 4. Notably in the (*Z*) isomer, the strongly negative charge on the carbonyl oxygen atom is less exposed to the environment, while those carbon atoms with a significant positive charge in both isomers appear to be slightly less positive in the (*E*) isomer. Also C23 is negative for the (*E*) and positive for the (*Z*) isomer, that is, in the (*Z*) isomer, the negative charge is less and the positive charge more localized and in the (*E*) isomer the opposite is true. The computed results reveal that only C1, C2, C5, C8, C11, C17, and C20 exhibit a positive Mulliken charge, whereas all other atoms exhibit

TABLE 1 Bond lengths (Å) by X-ray and theoretical calculations

	X-ray	B3LYP/6-31G(d,p). (E-isomer)
O(1)-C(1)	1.225(4)	1.240
O(2)-C(20)	1.361(4)	1.388
O(2)-C(23)	1.412(5)	1.452
N(1)-C(1)	1.356(5)	1.395
N(1)-C(8)	1.411(5)	1.410
N(1)-C(10)	1.461(5)	1.461
N(2)-C(2)	1.280(5)	1.288
N(2)-C(17)	1.419(4)	1.404
C(1)-C(2)	1.515(5)	1.523
C(2)-C(3)	1.460(5)	1.478
C(3)-C(8)	1.385(5)	1.419
C(3)-C(4)	1.402(5)	1.397
C(4)-C(5)	1.390(5)	1.407
C(5)-C(6)	1.394(5)	1.406
C(5)-C(9)	1.501(5)	1.513
C(6)-C(7)	1.384(5)	1.402
C(7)-C(8)	1.378(5)	1.390
C(10)-C(11)	1.503(5)	1.520

TABLE 2 Bond angles (°) by X-ray and theoretical calculations

	X-ray	DFT/B3LYP (E-isomer)
C(20)-O(2)-C(23)	118.3(4)	118.876
C(1)-N(1)-C(8)	110.7(3)	110.718
C(2)-N(2)-C(17)	120.7(3)	127.937
N(1)-C(1)-C(2)	106.5(3)	106.340
C(8)-C(3)-C(4)	119.4(3)	119.251
C(5)-C(4)-C(3)	119.7(3)	120.348
C(4)-C(5)-C(9)	121.4(3)	120.520
C(7)-C(6)-C(5)	122.2(4)	122.119
C(7)-C(8)-C(3)	122.0(3)	121.513
N(1)-C(10)-C(11)	113.7(3)	114.266

TABLE 3 Torsion angles (°) by X-ray and theoretical calculations

	X-ray	DFT/B3LYP (E-isomer)
C1-N1-C10-C11	−92.26	111.350
N1-C10-C11-C12	−123.61	128.804
N1-C10-C11-C16	56.99	−52.959
C3-C2-N2-C17	8.24	9.783
C22-C17-N2-C2	74.99	44.861

TABLE 4 Mulkin charges of the (*E*) and (Z) isomer

Atom	Mulliken E isomer	Mulliken Z isomer
C1	0.510	0.530
O1	−0.399	−0.413
C2	0.030	0.064
C3	0.084	0.064
C4	−0.131	−0.139
C5	0.08	0.085
C6	−0.156	−0.157
C7	−0.092	−0.094
C8	0.282	0.298
N1	−0.695	−0.713
N2	−0.340	−0.402
C10	−0.115	−0.185
C11	0.118	0.108
C12	−0.166	−0.140
C13	−0.125	−0.122
C14	−0.120	−0.116
C15	−0.128	−0.125
C16	−0.142	−0.128
C17	0.093	0.135
C18	−0.090	−0.054
H18	0.151	0.127
C19	−0.155	−0.134
C20	0.302	0.307
C21	−0.134	−0.153
C22	−0.096	−0.102
O2	−0.585	−0.584
C23	−0.54	0.154

negative charges. The maximum positive Mulliken charges were found on C1, C20, and C17 with 0.510, 0.302, and 0.093, respectively, because they are connected to more electronegative atoms. Interestingly, the N1 atom (−0.695) exhibits the maximum negative Mulliken charge. The generally more electronegative oxygen atoms O2 (−0.585) atom and O1 (−0.399) have intermediate negative Mulliken charges, while N2 (−0.340) has the least negative one of the heteroatoms. C5 and C8 are para-atoms of the indole's phenyl ring involved in the experimentally observed π-π stacking. The rings are twisted against each other so that the particularly positively charged atoms are not directly stacked but interact with atoms C4 and C7. The presence of a net positive charge on the hydrogen atom H18 (0.151) and the still

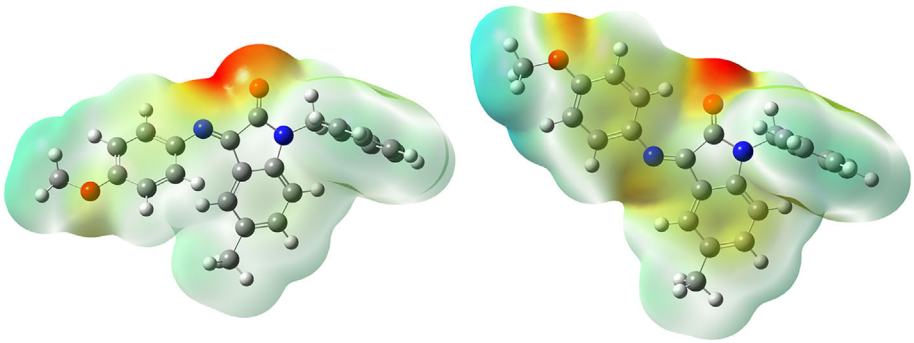

FIGURE 4 Calculated MEP surfaces of the (E) isomer (left) and the (Z) isomer (right) [Color figure can be viewed at wileyonlinelibrary.com]

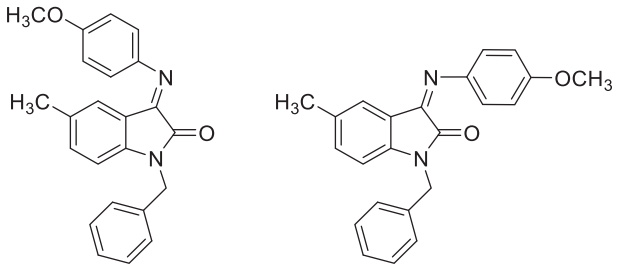

SCHEME 1 Chemical structures of the (*E*) and (*Z*) isomers

considerably negative charge on the adjacent nitrogen atom N2 (−0.340) could facilitate a charge transfer via the formation of the intermolecular hydrogen bond (C18—H18···N2) which was also observed experimentally.

2.2.2 | Molecule reactivity analysis by global reactivity descriptors

The frontier molecular orbitals (FMOs) comprise the highest energy–occupied molecular orbital (HOMO) and the lowest energy–unoccupied molecular orbital (LUMO) in a molecule, and these are the most important orbitals in a molecule as they define the compound's reactivity [15]. They are well-known indicators with respect to the reactivity of compounds as they determine the ability of a compound to accept an electron from (in the case of LUMO) or donate one to (in the case of HOMO) a reaction partner [16,17]. HOMO and LUMO orbitals of the (*E*) and (*Z*) isomer (see Scheme 1) of the title compound were examined and are shown in Figures 5 and 6.

The theoretical FMOs are further used for identifying the most likely origin and target atoms of intramolecular electron transfer from the highest occupied–molecular orbital (HOMO) to lowest unoccupied–molecular orbital (LUMO). The HOMO/LUMO energy gap constitutes a critical parameter in determining, for instance, molecular electrical transport properties [18,19]. The global chemical reactivity descriptors calculated for the (*E*) and (*Z*) isomer of the title compound using DFT are: electron affinity (A), chemical potential (μ), ionization potential (IP), chemical hardness (η), electronegativity (χ), and electrophilicity (ω), (Table 5) [20]. The calculated energy gap between HOMO and LUMO of the (*E*) isomer is 0.1132 Hartree (3.0811 eV), while for the (*Z*) isomer, it is larger with 0.12022 Hartree (3.2715 eV) demonstrating that the (*Z*) isomer is harder, more stable, and less reactive than the (*E*) isomer. The electron affinity (EA) reflects the change in the energy imposed on a species by receiving one additional electron, while the ionization potential (IP) value reflects the propensity of losing one electron. The chemical hardness (η) is a measure of mechanical deformation resistance or physical hardness. Essentially, it is the resistance measure against change in the electron distribution in a collection of nuclei and electrons [21]. From the global reactivity study, the HOMO and LUMO orbital energies lead to gas phase ionization energies (IP = −εHOMO) and electron affinities (EA = −εLUMO) of (*E*) and (*Z*) isomers of 5.4161/2.3350 eV and 5.5477/2.2762 eV. The electronegativity (χ) is a measure of the attraction of an atom for electrons in a covalent bond [22]. The computed electronegativity (χ = εHOMO + εLUMO)/2),) value for the (*E*) isomer is (2.708 eV) and for the (*Z*) isomer, it is (3.911 eV) indicating that the (*Z*) isomer has significantly greater electron accepting power than the (*E*) isomer. The global electrophilicity index ($\omega = \mu^2/2\,\eta$) was calculated using the electronic chemical potential (μ) and the chemical hardness (η). The global electrophilicity index (ω) reflects a compound's electrophilic power which depends on thermodynamic properties. It can be defined as the decrease in energy due to the flow of electrons from the donor (HOMO) to the acceptor (LUMO) in molecules. This plays an important role in determining the chemical reactivity of a system [23]. The electrophilicity values for the (*E*) and (*Z*) isomers are 4.871 eV and 4.677 eV, respectively, indicating that the (*E*) isomer is the stronger nucleophile while the (*Z*) isomer is the

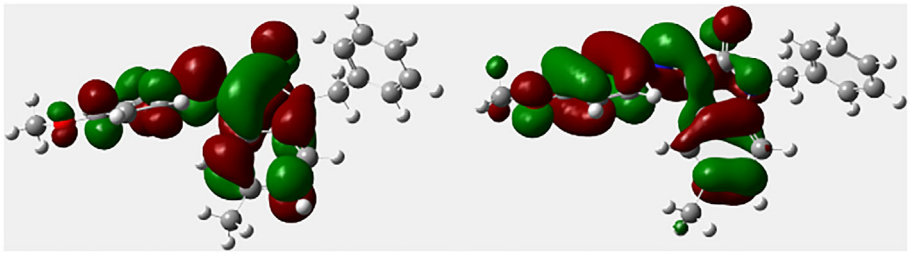

FIGURE 5 Plots of the frontier molecular orbitals for the (*E*) isomer; left: LUMO = −0.08581 Hartree = −2.3350 eV; right: HOMO = −0.19904 Hartree = −5.416 eV [Color figure can be viewed at wileyonlinelibrary.com]

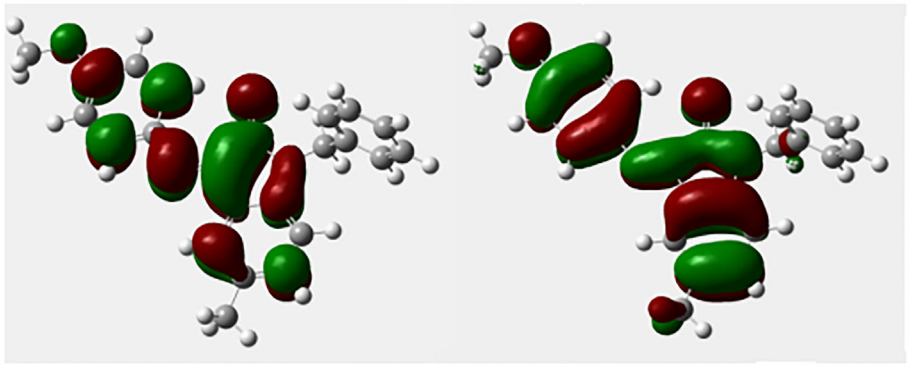

FIGURE 6 Plots of the frontier molecular orbitals for the (*Z*) isomer; left: LUMO = −0.08365 Hartree = −2.2762 eV; right: HOMO = −0.20387 Hartree = −5.5477 eV [Color figure can be viewed at wileyonlinelibrary.com]

TABLE 5 The calculated global reactivity properties of (*E*) and (*Z*) isomer by B3LYP/6-31G(d,p)

Parameter	E-isomer	Z-isomer
*E*HOMO (eV)	−5.4161 eV	−5.5477
*E*LUMO (eV)	−2.3350 eV	−2.2762
ΔE (eV)	3.0811	3.2715
IP (eV)	5.4161	5.5477
EA (eV)	2.3350	2.2762
Ƞ (eV)	1.5405	1.6357
χ (eV)	3.875	3.9119
ω (eV)	4.871	4.6778

stronger electrophile in accordance with the computed electronegativity [24–26]. Electrophilicity (ω) is used to describe the stabilization energy if the system subjected to saturation by electrons coming from the external environment. This reactivity information reveals whether or not a molecule can donate charge. A molecule with a low value of (ω) is a better nucleophile of higher reactivity, while higher values of (ω) indicate the presence of a good electrophile [22]. Our findings show that the (*Z*) isomer has lower values of (ω), indicating that it is the better nucleophile. Consequently, the (*E*) isomer appears to be the better electrophile. All of these values are substantially distinct for the two isomers which is surprising and highlights the importance of stereo-chemical factors for the reactivity of compounds. Finally, the total energy of each isomer was calculated and that of the (*E*) isomer (−1148.138 Hartree) appears to be slightly higher than that of the (*Z*) isomer (−1148.147 Hartree). Theoretically, the (Z) isomer is therefore more stable than the (*E*) isomer, but the observed difference (5.65 kcal·mol^{-1}) is not decisive enough to suggest that the formation of the (*E*) isomer is generally precluded. However, this energy difference contrasts the observation of the exclusive formation of the (*E*) isomer in the solid state. We therefore conclude that indeed the intermolecular interactions, in particular, the strong bifurcated hydrogen bond involving carbonyl oxygen and amine nitrogen as acceptors comprises the driving force for the exclusive formation of the (*E*) isomer in the crystalline material.

3 | CONCLUSION

It was possible to obtain a crystal structure of the known title compound in high quality. The metrical parameters are to some extent influenced by crystal packing effects and intermolecular interactions as confirmed by a computational analysis and respective observed differences in some distances and angles. Notably, the only experimentally observed isomer is not the thermodynamically favored one in the gas phase according to the computational evaluation. Parameters descriptive of the molecules' reactivity are distinct for

the two isomers. This study, thereby, highlights the relevance of isomerism which goes beyond merely geometrical/structural aspects with implications also for a pharmaceutical context in which the title compound and various derivatives thereof are being explored as well as the substantial impact crystal packing effects can have in the solid state.

4 | EXPERIMENTAL SECTION

4.1 | Physical techniques and materials

The reagents and solvents needed for synthesis and spectroscopic studies were commercially procured and used as received without further purification. NMR spectra were recorded on a Bruker spectrophotometer (400 MHz for ^{1}H and 100 MHz for ^{13}C), Faculty of Pharmacy, El-Mansoura University, El-Mansoura. Elemental analysis was performed on a Perkin Elmer 2400 CHN elemental analyzer, Regional Center for Mycology and Biotechnology, Al-Azhar University, Cairo, Egypt.

4.2 | Synthesis and characterization of (E)-1-benzyl-3-((4-methoxyphenyl)imino)-5-methylindolin-2-one

The synthesis of the known Schiff base compound (*E*)-1-benzyl-3-((4-methoxyphenyl)imino)-5-methylindolin-2-one according to literature procedures is outlined in Scheme 2. The first step involves the alkylation of 1*H*-indole-2,3-dione phenylbromide in DMF in the presence of K_2CO_3 as reported [23,27]. The second step comprises a typical Schiff base preparation using *p*-methoxyaniline in glacial acetic acid. These procedures were previously reported and discussed in detail by Wang et al. [28,29].

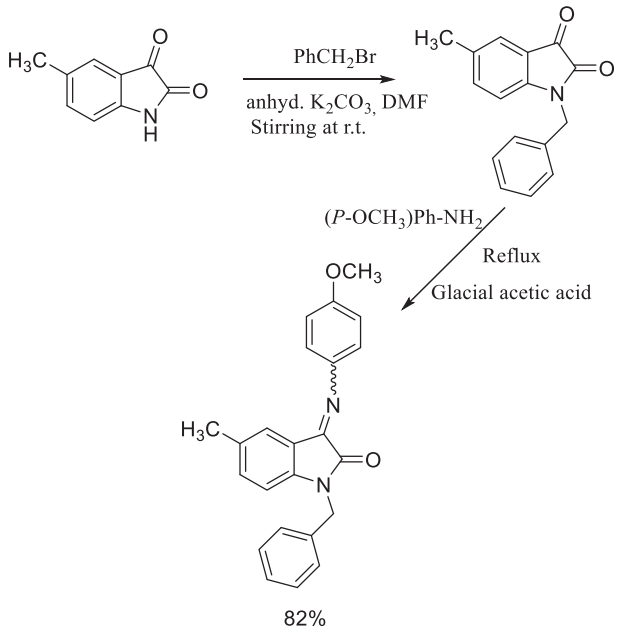

SCHEME 2 Two-step synthesis of the title compound

Elemental analysis for $C_{23}H_{20}N_2O_2$; calculated: C, 77.51; H, 5.66; N, 7.86. Found: C, 77.28; H, 5.89; N, 7.95.

H^1NMR: 7.41–7.31 (m, 2H, isatin), 7.19–7.29 (m, 2H, phenyl), 7.06–7.09 (m, 6H, benzyl), 6.91–6.95), 6.5 (singlet, 2H, $C\underline{H}_2$-benzyl, 3.3 (singlet, 3H, $OC\underline{H}_3$), 2.5 (triplet, 3H, $aC\underline{H}_3$).

C^{13}NMR: 163.03 (indole $\underline{C}$═O), 157.8 (indole $\underline{C}$═N), 153.95 ($\underline{C}$—OCH3), 145.04 (phenyl $\underline{C}$—N), 143.31, 141.40, 136.48, 134.79, 131.72, 129.19, 129.15, 128.01, 127.84, 127.79, 125.64, 123.63, 120.22, 115.96, 115.19, 113.93, 110.93 (Aro C), (55.77 ($O\underline{C}H_3$), 43.29 (benzyl $\underline{C}$—N), 20.98 (indole $\underline{C}H_3$).

4.3 | X-ray single crystal analysis

A suitable single crystal of compound I was mounted on a thin glass fiber which was coated with paraffin oil. X-ray single-crystal structural data were measured at low temperature (170 K) employing an STOE-IPDS II diffractometer that is equipped with a normal focus, 2.4 kW, sealed-tube X-ray source which generates graphite-monochromated Mo Kα radiation (λ = 0.71073 Å). The program XArea by STOE© was used for integrating the diffraction profiles. The structure was solved by direct methods with the programme SHELXT [30] and refined by full-matrix least-squares methods with the programme SHELXL [31]. All calculations were carried out with the WinGX system GUI, Ver 2018.3 [32]. Every non-hydrogen atom was refined anisotropically. All hydrogen atoms were located first on the density map and then refined isotropically on calculated positions using the typical riding model which constrains their U_{iso} values to $1.5U_{eq}$ of their pivot atoms for methyl groups and to $1.2U_{eq}$ of their pivot atoms for all other groups. Crystallographic data were deposited with the Cambridge Crystallographic Data Centre, CCDC, 12 Union Road, Cambridge CB21EZ, UK. These data can be obtained free of charge on quoting the depository number CCDC 2058589 by FAX (+44–1223–336-033), email (deposit@ccdc.cam.ac.uk) or, most conveniently, their web interface (at http://www.ccdc.cam.ac.uk).

Crystal and refinement data for the structure determination of compound (I) are summarized in Table 6.

TABLE 6 Crystallographic data of I crystallized as the (*E*) isomer

Empirical formula	$C_{23}\ H_{20}\ N_2\ O_2$
Formula weight	356.41
Temperature	170(2) K
Wavelength	0.71073 Å
Crystal system, space group	Orthorhombic, *Fdd*2
Unit cell dimensions	a = 48.727(10) Å, b = 8.7971(18) Å, c = 16.642(3) Å, α = β = γ = 90°
Volume	7134(2) $Å^3$
Z, calculated density	16, 1.327 g/cm^3
Absorption coefficient	0.085 mm^{-1}
F(000)	3008
Crystal size	0.196 × 0.137 × 0.116 mm^3
Theta range for data collection	3.345 to 29.498 deg.
Limiting indices	−66 < =h < =61, −12 < =k < =12, −21 < =l < =22
Reflections collected/unique	19,265/4780 [R(int) = 0.0753]
Completeness to theta = 25.242	99.8%
Absorption correction	None
Refinement method	Full-matrix least-squares on F^2
Data/restraints/parameters	4780/1/247
Goodness-of-fit on F^2	1.101
Final R indices[I > 2sigma(I)]	R1 = 0.0486, wR2 = 0.1091
R indices (all data)	R1 = 0.1011, wR2 = 0.1467
Absolute structure parameter	0.7(9)
Extinction coefficient	0.0026(3)
Largest diff. peak and hole	0.346 and − 0.309 e· $Å^{-3}$

4.4 | Quantum chemical calculations (DFT calculations)

DFT calculations were carried out with the Gaussian 09 W, and the data were analyzed with various methods [13,14,32–35]. For computational details (including a full list of co-authors) please refer to the Appendix S1.

DATA AVAILABILITY STATEMENT

The crystallographic data is stored with the CCDC and freely available after publication. The Cartesian coordinates of the computational investigation are supplied in the SI.

ORCID

Carola Schulzke https://orcid.org/0000-0002-7530-539X
Wesam S. Qayed https://orcid.org/0000-0001-7220-5628

REFERENCES

[1] L. H. Al-Wahaibi, J. Joubert, O. Blacque, N. H. Al-Shaalan, A. A. El-Emam, *Sci. Rep.* **2019**, *9*(1), 1.
[2] N. Karali, A. Gürsoy, F. Kandemirli, N. Shvets, F. B. Kaynak, S. Özbey, V. Kovalishyn, A. Dimoglo, *Bioorg. Med. Chem.* **2007**, *15*(17), 5888.
[3] P. Mondal, M. Banerjee, S. Jana, A. Bose, *J. Young Pharm.* **2010**, *2*(2), 169.
[4] V. Asati, S. K. Bharti, *J. Mol. Struct.* **2018**, *1154*, 406.
[5] A. Carreño, C. Zúñiga, D. Páez-Hernández, M. Gacitúa, R. Polanco, C. Otero, R. Arratia-Pérez, J. A. Fuentes, *New J. Chem.* **2018**, *42*(11), 8851.
[6] A. D. Khalaji, H. Mighani, M. Kazemnejadi, K. Gotoh, H. Ishida, K. Fejfarova, M. Dusek, *Arab. J. Chem.* **2017**, *10*, S1808–S1813.
[7] K. Somarathinam, S. Velautham, R. Perumal, S. Kandasamy, S. Srinivasan, E. Gayathri, G. Kothandan, S. Usharani, *Chem. Data Collect.* **2019**, *21*, 100227.
[8] S. J. Y. Macalino, J. B. Billones, V. G. Organo, M. C. O. Carrillo, *Molecules* **2020**, *25*(3), 1.
[9] E. A. Hassan, N. Nawar, M. M. Mostafa, *Appl. Organomet. Chem.* **2019**, *33*(9), 1.
[10] I. Sheikhshoaie, H. Stoeckli-Evans, A. Akbari, S. Ali Yasrebi, S. Y. Ebrahimipour, *Arab. J. Chem.* **2012**, *5*(2), 173.
[11] O. Engkvist, P.-O. Norrby, N. Selmi, Y.-h. Lam, Z. Peng, E. C. Sherer, W. Amberg, T. Erhard, L. A. Smyth, *Drug Discov. Today* **2018**, *23*(6), 1203.
[12] R. L. Araújo, M. S. Vasconcelos, C. A. Barboza, J. X. Lima Neto, E. L. Albuquerque, U. L. Fulco, *Comput. Theor. Chem.* **2019**, *1170*, 112621.
[13] R. S. Mulliken, *J. Chem. Phys.* **1955**, *28*, 1833.
[14] P. Sivajeyanthi, B. Edison, K. Balasubramani, G. Premkumar, T. Swu, *Acta Crystallogr. Sect. E Crystallogr. Commun.* **2019**, *75*, 804.
[15] M. S. H. Faizi, M. N. Lone, N. Dege, S. Malinkin, T. Y. Sliva, *Acta Crystallogr. Sect. E Crystallogr. Commun.* **2018**, *74*, 1540.
[16] F. Güntepe, H. Saraçoglu, N. Çaliskan, Ç. Yüksektepe, A. Çukurovali, *J. Struct. Chem.* **2011**, *52*(3), 596.
[17] C. Cojocaru, A. Airinei, N. Fifere, *Springerplus* **2013**, *2*(1), 1.
[18] N. A. Ancın, S. G. Öztaş, Ö. Küçükterzi, N. A. Öztaş, *J. Mol. Struct.* **2019**, *1198*, 126868.
[19] M. E. M. O. O. E. Ebenso, *J. Mol. Struct.* **2017**, *1136*, 127.
[20] A. M. Oklje, O. R. Klisuri, *J. Mol. Struct.* **2021**, *1226*, 129341.
[21] R. G. Pearson, *J. Chem. Sci.* **2005**, *117*(5), 369.
[22] M. Miar, A. Shiroudi, K. Pourshamsian, A. R. Oliaey, F. Hatamjafari, *J. Chem. Res.* **2021**, *45*, 147.
[23] Q. Guo, Y. Liu, X. Li, L. Zhong, Y. Peng, *J. Org. Chem.* **2012**, *77*, 3589.
[24] S. R. Hussaini, A. Kuta, A. Pal, Z. Wang, M. A. Eastman, R. Duran, *ACS Omega* **2020**, *5*, 24848–24853.
[25] R. Giaser, *Magn. Reson. Chem.* **1991**, *29*, 766.
[26] L. R. Domingo, *Molecules* **2016**, *1*, 1.
[27] C.-G. Y. Hong Gao, J. Sun, *J. Org. Chem.* **2014**, *9*, 4131.
[28] Y. M. Wang, H. H. Zhang, C. Li, T. Fan, F. Shi, *Chem. Commun.* **2016**, *52*(9), 1804.

[29] H. H. Zhang, X. X. Sun, J. Liang, Y. M. Wang, C. C. Zhao, F. Shi, *Org. Biomol. Chem.* **2014**, *12*(47), 9539.
[30] G. M. Sheldrick, *Acta Cryst. A* **2015**, *71*, 3.
[31] G. M. Sheldrick, *Acta Cryst. C* **2014**, *71*, 3.
[32] L. J. Farrugia, *J. Appl. Crystallogr.* **2012**, *45*, 849.
[33] H. B. Schlegel, *J. Comput. Chem.* **1982**, *3*(2), 214.
[34] M. M. J. Frisch, G. W. Trucks, H. B. Schlegel, G. E. Scuseria, M. A. Robb, J. R. Cheeseman, G. Scalmani, V. Barone, G. A. Petersson, H. Nakatsuji, X. Li, M. Caricato, A. Marenich, J. Bloino, B. G. Janesko, R. Gomperts, B. Mennucci, H. P. Hratchian, J. V. Ortiz, A. F. Izmaylov, J. L. Sonnenberg, D. Williams-Young, F. Ding, F. Lipparini, F. Egidi, J. Goings, B. Peng, A. Petrone, T. Henderson, D. Ranasinghe, V. G. Zakrzewski, J. Gao, N. Rega, G. Zheng, W. Liang, M. Hada, M. Ehara, K. Toyota, R. Fukuda, J. Hasegawa, M. Ishida, T. Nakajima, Y. Honda, O. Kitao, H. Nakai, T. Vreven, K. Throssell, J. A. Montgomery, Jr., J. E. Peralta, F. Ogliaro, M. Bearpark, J. J. Heyd, E. Brothers, K. N. Kudin, V. N. Staroverov, T. Keith, R. Kobayashi, J. Normand, K. Raghavachari, A. Rendell, J. C. Burant, S. S. Iyengar, J. Tomasi, M. Cossi, J. M. Millam, M. Klene, C. Adamo, R. Cammi, J. W. Ochterski, R. L. Martin, K. Morokuma, O. Farkas, J. B. Foresman, D. J. Fox. Gaussian 09, Revision D.01. **1998**.
[35] W. Guerrab, H. Lgaz, S. Kansiz, J. T. Mague, N. Dege, M. Ansar, R. Marzouki, J. Taoufik, I. H. Ali, I.-M. Chung, Y. Ramli, *J. Mol. Struct.* **2020**, *1205*, 1425.

SUPPORTING INFORMATION

Additional supporting information may be found online in the Supporting Information section at the end of this article.

How to cite this article: H. A. A. Abdel El-wahab, A. K. Hamdy, C. Schulzke, T. Aboul-Fadl, W. S. Qayed, *J Heterocyclic Chem* **2021**, 1. https://doi.org/10.1002/jhet.4284